# Signature of Primordial Non-Gaussianity on Matter Power Spectrum

Atsushi Taruya[1,2], Kazuya Koyama[3], Takahiko Matsubara[4]

[1] *Research Center for the Early Universe, School of Science, University of Tokyo, Bunkyo-ku, Tokyo 113-0033, Japan*

[2] *Institute for the Physics and Mathematics of the Universe, University of Tokyo, Kashiwa, Chiba 277-8568, Japan*

[3] *Institute of Cosmology & Gravitation, University of Portsmouth, Portsmouth, Hampshire, PO1 2EG, UK and*

[4] *Department of Physics, Nagoya University, Chikusa-ku, Nagoya 464-8602, Japan*

(Dated: December 25, 2008)

Employing the perturbative treatment of gravitational clustering, we discuss possible effects of primordial non-Gaussianity on the matter power spectrum. As gravitational clustering develops, the coupling between different Fourier modes of density perturbations becomes important and the primordial non-Gaussianity which intrinsically possesses a non-trivial mode-correlation can affect the late-time evolution of the power spectrum. We quantitatively estimate the non-Gaussian effect on power spectrum from the perturbation theory. The potential impact on the cosmological parameter estimation using the power spectrum are investigated based on the Fisher-matrix formalism. In addition, on the basis of the local biasing prescription, non-Gaussian effects on the galaxy power spectrum are considered, showing that the scale-dependent biasing arises from a local-type primordial non-Gaussianity. On the other hand, an equilateral-type non-Gaussianity does not induce such scale-dependence because of weaker mode-correlations between small and large Fourier modes.

PACS numbers: 98.80.-k



## I. INTRODUCTION

Recent observations of cosmic microwave background (CMB) anisotropies as well as density perturbations in the large-scale structure strongly support the basic predictions of inflationary scenarios, in which primordial adiabatic fluctuations were produced during the accelerated phase of the cosmic expansion and their statistical properties are approximately described by Gaussian statistics with a nearly scale-invariant power spectrum (e.g., [33, 68]). Some specific inflationary models have been ruled out by observations, narrowing the constraints on the early stage of the universe. With precision measurements from future observations, we will detect clear signals that help us to discriminate between many candidate of inflationary models.

Amongst several signals accessible in the near future, departure from Gaussianity is an important clue to probe the generation mechanism for primordial perturbations as well as to discriminate between inflation models. While the simplest slow-roll inflation with single scalar field predicts a small departure from Gaussianity (e.g., [1, 11, 41]), models with a non-trivial kinetic term or late-time inflaton decay called curvaton scenario [37, 48] can produce a large non-Gaussianity (e.g., [8, 38, 55, 58]). There are also viable models motivated by string theory that produce large non-Gaussianity such as Dirac-Born-Infeld (DBI) inflation [4, 6, 7, 15, 28, 28, 35] and ekyprotic scenario [13, 18, 32, 34, 36]. Although tentative detections of primordial non-Gaussianity have been reported very recently ([47, 69], but see also [26, 33]) and the result is broadly consistent with the standard prediction of slow-roll inflation, these detections are at relatively low statistical significance and more precise measurements are necessary for a definite detection of the non-Gaussian signals. Planned CMB surveys, namely the Planck mission [52], will have much greater sensitivity and better detect non-Gaussian signals (e.g., [61]). Further, large-scale structure data from future spectroscopic surveys will uncover the mass density fluctuations up to Giga parsec scales, which preserve the statistical properties of primordial fluctuations (e.g., [57, 59]). Since these two measurements can probe different scales of primordial fluctuations, they are, in principle, complementary to each other.

In the present paper, we study the signature of primordial non-Gaussianity imprinted on the large-scale structure, especially focusing on the matter power spectrum. Naively, we expect that the signature of primordial non-Gaussianity basically appears in the statistical properties of higher-order quantities such as the bispectrum and trispectrum, and the power spectrum as a second-order statistic remains unchanged even if large non-Gaussianity has been produced. However, this is true only when the fluctuations of the mass density field are tiny and well within the linear regime. As the gravitational clustering develops, the coupling between different Fourier modes becomes important and the scale-dependent non-linear growth appears due to the mode-coupling effect. In the weakly non-linear regime, the

strength of this mode-coupling sensitively depends on the initial condition. Since the non-Gaussian density field intrinsically possesses non-trivial mode-correlations, the evolution of the power spectrum may be altered by the primordial non-Gaussianity, at least in the weakly non-linear regime.

Here, employing the perturbative calculations, we study the effect of primordial non-Gaussianity on the matter power spectrum. The effect of non-Gaussianity on the matter power spectrum has been previously investigated by Ref.[57] using perturbation theory, showing that the magnitude of this effect is roughly at the few percent level in the weakly non-linear regime. In this paper, adopting the two representative models of primordial non-Gaussianity described in Sec. II, we quantitatively estimate the non-Gaussian effects on the power spectrum and elucidate their shape dependence (Sec. III). In particular, we carefully examine the influence of primordial non-Gaussianity on cosmological parameter estimation, paying particular attention to the primordial spectral indices and the characteristic scale of the baryon acoustic oscillations as a cosmic standard ruler (Sec. IV). Also, we discuss the non-Gaussian effect on the galaxy biasing (Sec. V). This issue has been recently studied by several authors in the context of the halo biasing prescription [2, 19, 42, 46, 62], and local biasing prescription [46]. Here, we adopt the local biasing scheme and consider the scale-dependent galaxy biasing arising from the primordial non-Gaussianity.

Throughout the paper, we assume a flat Lambda cold dark matter (CDM) model and the fiducial model parameters are chosen based on the five-year WMAP results (WMAP+BAO+SN ML, see Ref.[33]): $\Omega_{\rm b}h^2 = 0.02263$, $\Omega_{\rm c}h^2 = 0.1136$, $\Omega_{\rm K} = 0$ ($\Omega_\Lambda = 0.724$), $n_s = 0.961$, $\tau = 0.080$, $\Delta_{\mathcal{R}}(k = 0.002{\rm Mpc}^{-1}) = 2.42 \times 10^{-9}$, $h = 0.703$.

## II. PRIMORDIAL NON-GAUSSIANITY

According to the commonly accepted mechanisms to generate the primordial fluctuations, non-Gaussianity would be imprinted on the primordial curvature perturbation produced during inflation. The curvature perturbation can also be generated after inflation by a late-time decay of light fields, and this would produce a large non-Gaussianity in the curvature perturbation. Further, as alternative scenarios to inflation such as ekpyrotic models, nearly scale-invariant curvature perturbation with large non-Gaussianity could be generated during the collapsing phase of the Universe.

Let us denote the primordial curvature perturbation on the uniform density hypersurface and the Bardeen's curvature potential at super-horizon scales by $\zeta_p$ and $\Phi_{H,p}$, respectively. The primordial density perturbation defined at an early time of the matter dominated epoch, $\delta_0$, is related to these variables through (e.g., [25, 39, 57, 59])

$$\delta_0(\boldsymbol{k}) = M_\zeta(k)\zeta_p(\boldsymbol{k}) = \frac{5}{3}M_\zeta(k)\Phi_{H,p}(k), \tag{2.1}$$

with the function $M_\zeta$ being

$$M_\zeta(k) = \frac{2}{5}\frac{k^2\,T(k)}{\Omega_{\rm m,0}H_0^2}, \tag{2.2}$$

where the function $T(k)$ is the transfer function of matter fluctuations normalized to unity at $k \to 0$. Note that the curvature potential given in the matter dominated epoch, $\Phi_{H,p}$, is related to the curvature perturbation $\zeta(\boldsymbol{k}) = (5/3)\,\Phi_{H,p}(\boldsymbol{k})$.

Using the relation (2.1), $n$-point statistics of the primordial density field are all expressed in terms of respective correlator of the curvature potential or the curvature perturbation. For the power spectra, we have

$$P_0(k) = M_\zeta^2(k)\,P_\zeta(k), \tag{2.3}$$

with quantities $P_0$ and $P_\zeta$ defined by

$$\langle\delta_0(\boldsymbol{k})\delta_0(\boldsymbol{k}')\rangle = (2\pi)^3\delta_{\rm D}(\boldsymbol{k}+\boldsymbol{k}')\,P_0(k), \quad \langle\zeta_p(\boldsymbol{k})\zeta_p(\boldsymbol{k}')\rangle = (2\pi)^3\delta_{\rm D}(\boldsymbol{k}+\boldsymbol{k}')\,P_\zeta(k). \tag{2.4}$$

The bispectrum as the first non-trivial quantity arising from the non-Gaussianity becomes

$$B_0(\boldsymbol{k}_1,\boldsymbol{k}_2,\boldsymbol{k}_3) = M_\zeta(k_1)M_\zeta(k_2)M_\zeta(k_3)\;B_\zeta(\boldsymbol{k}_1,\boldsymbol{k}_2,\boldsymbol{k}_3), \tag{2.5}$$

where we define

$$\begin{aligned}\Big\langle\delta_0(\boldsymbol{k}_1)\delta_0(\boldsymbol{k}_2)\delta_0(\boldsymbol{k}_3)\Big\rangle &= (2\pi)^3\,\delta_{\rm D}(\boldsymbol{k}_1+\boldsymbol{k}_2+\boldsymbol{k}_3)\,B_0(\boldsymbol{k}_1,\boldsymbol{k}_2,\boldsymbol{k}_3),\\ \Big\langle\zeta_p(\boldsymbol{k}_1)\zeta_p(\boldsymbol{k}_2)\zeta_p(\boldsymbol{k}_3)\Big\rangle &= (2\pi)^3\,\delta_{\rm D}(\boldsymbol{k}_1+\boldsymbol{k}_2+\boldsymbol{k}_3)\,B_\zeta(\boldsymbol{k}_1,\boldsymbol{k}_2,\boldsymbol{k}_3).\end{aligned} \tag{2.6}$$

Details of the functional form of $B_\zeta$ depend on the generation mechanism of primordial non-Gaussianity. In the following, we will consider two representative models of non-Gaussianity and give the explicit expressions for the primordial bispectrum $B_\zeta$.

### A. Local model

In the local model of primordial non-Gaussianity, the primordial fluctuation $\Phi_{H,p}$ is characterized by the Taylor expansion of the Gaussian field. Denoting the Gaussian field by $\varphi$, it is conventionally characterized as:

$$\Phi_{H,p}(\boldsymbol{x}) = \varphi(\boldsymbol{x}) + f_{\rm NL}\left\{\varphi^2(\boldsymbol{x}) - \langle\varphi^2\rangle\right\} + \cdots . \tag{2.7}$$

The Fourier counterpart of the above equation is given by

$$\Phi_{H,p}(\boldsymbol{k}) = \varphi(\boldsymbol{k}) + f_{\rm NL}\int\frac{d^3\boldsymbol{q}}{(2\pi)^3}\left\{\varphi(\boldsymbol{q})\varphi(\boldsymbol{k}-\boldsymbol{q}) - \langle\varphi(\boldsymbol{q})\varphi(\boldsymbol{k}-\boldsymbol{q})\rangle\right\} + \cdots . \tag{2.8}$$

Alternatively, we can expand $\zeta_p$ as:

$$\zeta_p(\boldsymbol{k}) = \zeta_{\rm G}(\boldsymbol{k}) + \frac{3}{5}f_{\rm NL}\int\frac{d^3\boldsymbol{q}}{(2\pi)^3}\left\{\zeta_{\rm G}(\boldsymbol{q})\zeta_G(\boldsymbol{k}-\boldsymbol{q}) - \langle\zeta_{\rm G}(\boldsymbol{q})\zeta_{\rm G}(\boldsymbol{k}-\boldsymbol{q})\rangle\right\} + \cdots , \tag{2.9}$$

where $\zeta_{\rm G}$ is Gaussian field and we have the relation $\zeta_{\rm G} = (5/3)\varphi$. For the cases of interest here, deviation from Gaussianity is generally small and perturbative evaluation of the primordial bispectrum is valid. The leading-order result becomes

$$B_\zeta(\boldsymbol{k}_1,\boldsymbol{k}_2,\boldsymbol{k}_3) \simeq \frac{6}{5}f_{\rm NL}\Big[P_\zeta(k_1)P_\zeta(k_2) + P_\zeta(k_2)P_\zeta(k_3) + P_\zeta(k_3)P_\zeta(k_1)\Big]. \tag{2.10}$$

In the slow-roll inflation models, $f_{\rm NL}$ is suppressed by the slow-roll parameters and thus it is expected to be very small. However, in curvaton models or ekpyrotic models, it is possible to generate a large non-Gaussianity of the local model with $f_{\rm NL}\sim\mathcal{O}(10^2)$.

### B. Equilateral model

As another type of bispectrum configuration, we consider an equilateral model. The DBI inflation is a typical example where the bispectrum has a maximum amplitude for equilateral configurations. This is in contrast with the local model where the bispectrum has the largest amplitude for squeezed configurations [9]. The bispectrum in the equilateral model is approximated by [17][1]

$$\begin{aligned} B_\zeta(\boldsymbol{k}_1,\boldsymbol{k}_2,\boldsymbol{k}_3) \;=\; \frac{18}{5}\,f_{\rm NL}^{\rm eq}\left(\frac{\bar{k}}{k_{\rm CMB}}\right)^{-2\kappa} & \Big[-P_\zeta(k_1)P_\zeta(k_2) - P_\zeta(k_2)P_\zeta(k_3) - P_\zeta(k_3)P_\zeta(k_1) \\ & -2\left\{P_\zeta(k_1)P_\zeta(k_2)P_\zeta(k_3)\right\}^{2/3} + \left\{\left(P_\zeta(k_1)\{P_\zeta(k_2)\}^2\{P_\zeta(k_3)\}^3\right)^{1/3} + (5\text{ perm.})\right\}\Big], \end{aligned} \tag{2.11}$$

with $\bar{k} = (k_1+k_2+k_3)/3$. Here, we introduce the slope index $\kappa$ in order to characterize the scale-dependence of the non-Gaussianity, which generically appears in the DBI-type inflation models. we set the characteristic scale to $k_{\rm CMB} = 0.04\,{\rm Mpc}^{-1}$. Note that the bispectrum in equation (2.11) is normalized in such a way that, for equilateral configurations ($k_1 = k_2 = k_3 = k$), it coincides with the local form given in equation (2.10).

## III. NON-LINEAR EVOLUTION OF MATTER POWER SPECTRUM FROM PERTURBATION THEORY

### A. Perturbation Theory

Even if the primordial fluctuations are well described by linear theory, the non-linearity of the gravitational dynamics eventually dominates and we must correctly take into account the non-linear growth of matter fluctuations, which

[1] The expression given here is slightly generalized in a sense that we do not necessarily assume a power-law form of the power spectrum, $P_\zeta(k)$.

significantly modifies the matter power spectrum. For the scales of interest here, especially the accessible scales of future galaxy redshift surveys, the non-linear evolution is rather moderate and perturbative treatment is valid. The mass density field is described by

$$\delta(\boldsymbol{k};z) = \delta^{(1)}(\boldsymbol{k};z) + \delta^{(2)}(\boldsymbol{k};z) + \delta^{(3)}(\boldsymbol{k};z) + \cdots . \tag{3.1}$$

In the above, the function $\delta^{(1)}(\boldsymbol{k};z)$ represents the linear fluctuation and it is given by $\delta^{(1)}(\boldsymbol{k};z) = D(z)\delta_0(\boldsymbol{k})$, where $D(z)$ is the linear growth rate. Neglecting the decaying mode of linear perturbation, the solutions for higher-order quantities are formally expressed as [12]

$$\delta^{(n)}(\boldsymbol{k};z) = [D(z)]^n \int \frac{d^3k_1\cdots d^3k_n}{(2\pi)^{3(n-1)}}\,\delta_{\rm D}(\boldsymbol{k}-\boldsymbol{k}_1-\cdots-\boldsymbol{k}_n)\,F^{(n)}_{\rm sym}(\boldsymbol{k}_1,\cdots,\boldsymbol{k}_n)\delta_0(\boldsymbol{k}_1)\cdots\delta_0(\boldsymbol{k}_n), \tag{3.2}$$

with $F^{(n)}_{\rm sym}$ being the symmetrized kernel for the $n$-th order solution. Then, the power spectrum of the density field, defined as

$$\langle\delta(\boldsymbol{k};z)\delta(\boldsymbol{k}';z)\rangle = (2\pi)^3\delta_{\rm D}(\boldsymbol{k}+\boldsymbol{k}')\;P(k;z), \tag{3.3}$$

can be calculated by substituting Eq.(3.2) into the above expression. The resultant expression is summarized as

$$P(k;z) = D^2(z)\,P_0(k) + P^{(12)}(k;z) + \Big[\,P^{(22)}(k;z) + P^{(13)}(k;z)\,\Big] + \cdots , \tag{3.4}$$

where the terms $P^{(12)}$, $P^{(22)}$ and $P^{(13)}$ are the so-called one-loop power spectra given by

$$P^{(12)}(k;z) \;=\; 2\,D^3(z)\int\frac{d^3q}{(2\pi)^3}\,F^{(2)}_{\rm sym}(\boldsymbol{q},\boldsymbol{k}-\boldsymbol{q})\,B_0(-\boldsymbol{k},\boldsymbol{q},\boldsymbol{k}-\boldsymbol{q}), \tag{3.5}$$

$$\begin{aligned} P^{(22)}(k;z) \;=\;& 2\,D^4(z)\int\frac{d^3q}{(2\pi)^3}\,\{\,F^{(2)}_{\rm sym}(\boldsymbol{q},\boldsymbol{k}-\boldsymbol{q})\,\}^2\,P_0(q)P_0(|\boldsymbol{k}-\boldsymbol{q}|) \\ &+D^4(z)\int\frac{d^3pd^3q}{(2\pi)^6}\,F^{(2)}_{\rm sym}(\boldsymbol{p},\boldsymbol{k}-\boldsymbol{p})F^{(2)}_{\rm sym}(\boldsymbol{q},-\boldsymbol{k}-\boldsymbol{q})\,T_0(\boldsymbol{p},\boldsymbol{k}-\boldsymbol{p},\boldsymbol{q},-\boldsymbol{k}-\boldsymbol{q}), \end{aligned} \tag{3.6}$$

$$\begin{aligned} P^{(13)}(k;z) \;=\;& 6\,D^4(z)\int\frac{d^3q}{(2\pi)^3}\,F^{(3)}_{\rm sym}(\boldsymbol{k},\boldsymbol{q},-\boldsymbol{q})\,P_0(k)P_0(q) \\ &+2\,D^4(z)\int\frac{d^3pd^3q}{(2\pi)^6}\,F^{(3)}_{\rm sym}(\boldsymbol{p},\boldsymbol{q},\boldsymbol{k}-\boldsymbol{p}-\boldsymbol{q})\,T_0(-\boldsymbol{k},\boldsymbol{p},\boldsymbol{q},\boldsymbol{k}-\boldsymbol{p}-\boldsymbol{q}). \end{aligned} \tag{3.7}$$

These are the most general expressions for the one-loop power spectra in the presence of primordial non-Gaussianity. The quantity $P^{(12)}$ is the first non-trivial correction associated with the primordial density bispectrum $B_0(\boldsymbol{k}_1,\boldsymbol{k}_2,\boldsymbol{k}_3)$. While the quantities $P^{(22)}$ and $P^{(13)}$ represent the first leading-order corrections in the case of Gaussian initial conditions, additional contributions originating from the primordial density trispectrum, $T_0(\boldsymbol{k}_1,\boldsymbol{k}_3,\boldsymbol{k}_3,\boldsymbol{k}_4)$, also arise. Thus, in general, we need the explicit functional form of the primordial trispectrum as well as primordial bispectrum in order to compute the one-loop power spectra. However, in most general cases, the primordial trispectrum is of the order of $M_\zeta^4P_0^3$, which is negligibly smaller than the bispectrum, $B_0\sim M_\zeta^3P_0^2$. Since the terms including $P_0^3$ may be regarded as the two-loop order, we can safely neglect the trispectrum contribution. With this treatment, the terms $P^{(22)}$ and $P^{(13)}$ reduce to nothing but the *standard* one-loop spectra, and they are explicitly given by (e.g., [29, 40, 49, 56])

$$P^{(22)}(k;z) \;=\; D^4(z)\,\frac{k^3}{(2\pi)^2}\int_0^\infty dx\,x^2P_0(kx)\int_{-1}^{+1}d\mu\,P_0\left(k\sqrt{1+x^2-2\mu\,x}\right)\,\frac{1}{2}\left[\frac{3x+7\mu-10\mu^2x}{7x(1+x^2-2\mu x)}\right]^2, \tag{3.8}$$

$$\begin{aligned} P^{(13)}(k;z) \;=\;& D^4(z)\,\frac{k^3}{(2\pi)^2}\,P_0(k)\int_0^\infty dx\,x^2P_0(kx) \\ &\times\,\frac{1}{252\,x^2}\left[\frac{12}{x^2}-158+100x^2-42x^4+\frac{3}{x^3}\,(x^2-1)^3(7x^2+2)\,\ln\left|\frac{x+1}{x-1}\right|\right]. \end{aligned} \tag{3.9}$$

Also, the non-trivial contribution from the primordial bispectrum is expressed in terms of the bispectrum of the curvature perturbation as

$$\begin{aligned} P^{(12)}(k;z) \;=\;& D^3(z)\,\frac{k^3}{(2\pi)^2}\int_0^\infty dx x^2\int_{-1}^{+1}d\mu\,\frac{3x+7\mu-10\mu^2\,x}{7x(1+x^2-2\mu\,x)} \\ &\times\,M_\zeta(k)M_\zeta(kx)M_\zeta(k\sqrt{1+x^2-2\mu x})\;B_\zeta(k,kx,k\sqrt{1+x^2-2\mu x}). \end{aligned} \tag{3.10}$$

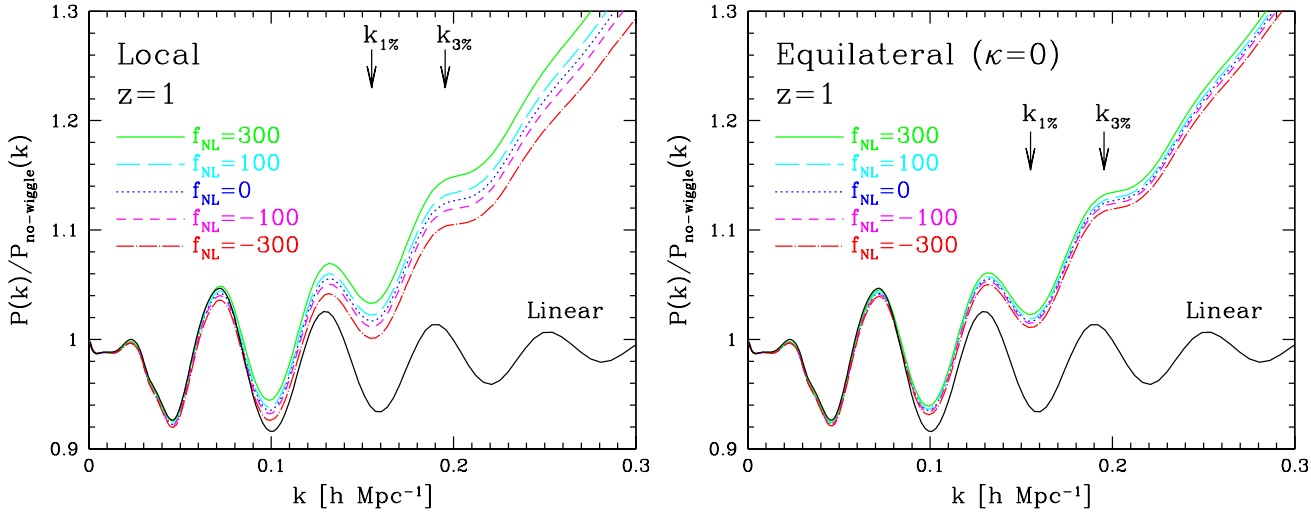


FIG. 1: Ratio of the power spectrum to the smoothed reference spectrum for the local model (left) and the equilateral model with $\kappa = 0$ (right), for $z = 1$. The smooth spectra are obtained from the no-wiggle approximation of the linear transfer function according to Ref. [20]. The lines from top to bottom respectively indicate $f_{\rm NL} = 300$ (solid), $f_{\rm NL} = 100$ (long-dashed), $f_{\rm NL} = 0$ (dotted), $f_{\rm NL} = -100$ (short-dashed) and $f_{\rm NL} = -300$ (dot-dashed).

### B. Results

Based on the expressions given above, we now calculate the matter power spectrum, focusing on the scales relevant for future galaxy surveys. Figure 1 plots the ratios of power spectra to the smooth reference spectrum, $P(k)/P_{\rm no\text{-}wiggle}(k)$, given at $z = 1$. The reference spectrum $P_{\rm no\text{-}wiggle}(k)$ is the linear power spectra computed from the no-wiggle approximation of the transfer function given by Ref. [20]. The left panel shows the results for the local model, and the right panel plots the results for the equilateral model with index $\kappa = 0$. The overall behavior at higher $k$ is basically dominated by the corrections coming from the standard 1-loop power spectra, $P^{(22)}$ and $P^{(13)}$, but small variation of the power spectrum amplitudes manifests at higher $k$. This is the contribution of primordial non-Gaussianity, $P^{(12)}$, originating from the primordial bispectrum. Depending on the sign of $f_{\rm NL}$, the primordial non-Gaussianity enhances or suppresses the non-linear growth of the power spectrum and the deviation from the Gaussian result ($f_{\rm NL} = 0$) becomes more significant as $|f_{\rm NL}|$ increases. Although the effect of primordial non-Gaussianity seems rather mild within the current constrained values of $-9 \lesssim f_{\rm NL}^{\rm local} \lesssim 111$ and $-151 \lesssim f_{\rm NL}^{\rm eq} \lesssim 253$ (95%C.L.)[33], we do not immediately exclude the possibility of significant impact on the cosmological parameter estimation. We will discuss this issue in the next section.

Next we will focus on the shape of the power spectrum. In Figure 2, the ratios of the power spectra to those in the Gaussian case ($f_{\rm NL} = 0$), i.e., $P(k; f_{\rm NL} \neq 0)/P(k; f_{\rm NL} = 0)$, are plotted for various redshifts and values of $f_{\rm NL}$. Note that in computing the ratio, both the numerator and denominator are calculated from perturbation theory. In Figures 1 and 2, the vertical arrows labeled by $k_{1\%}$ and $k_{3\%}$ indicate the maximum wavenumber below which the precision level of perturbation theory prediction is expected to be better than 1% and 3%, respectively. According to recent numerical experiments, the maximum wavenumber is empirically determined through [50]

$$k^2 \int_0^k \frac{dq}{6\pi^2} D^2(z) P_0(q) = C, \tag{3.11}$$

where $C = 0.18$ (0.3) for $k_{1\%}$ ($k_{3\%}$). Solving the above equation with respect to $k$, we obtain $k_{1\%}$ and $k_{3\%}$ as function of redshift. Note that the maximum wave numbers given above have been derived by comparison between N-body simulations and theoretical predictions, and the resultant convergence range is narrower than those previously proposed (e.g., [30, 59]). In this sense, Eq.(3.11) may be regarded as a conservative criterion.

Bearing the limitation of perturbation theory in mind, we see that the deviation of the power spectrum from the Gaussian case also depends on the redshift and scales as well as the model of primordial non-Gaussianity. Monotonic change of the power spectrum amplitude is broadly consistent with recent N-body simulations in the case of the local model [23], although the fractional change is typically $\lesssim 2 - 3\%$, as expected from Figure 1. Note, however, that the level of this changes roughly corresponds to the sensitivity achievable with future redshift surveys. As references,

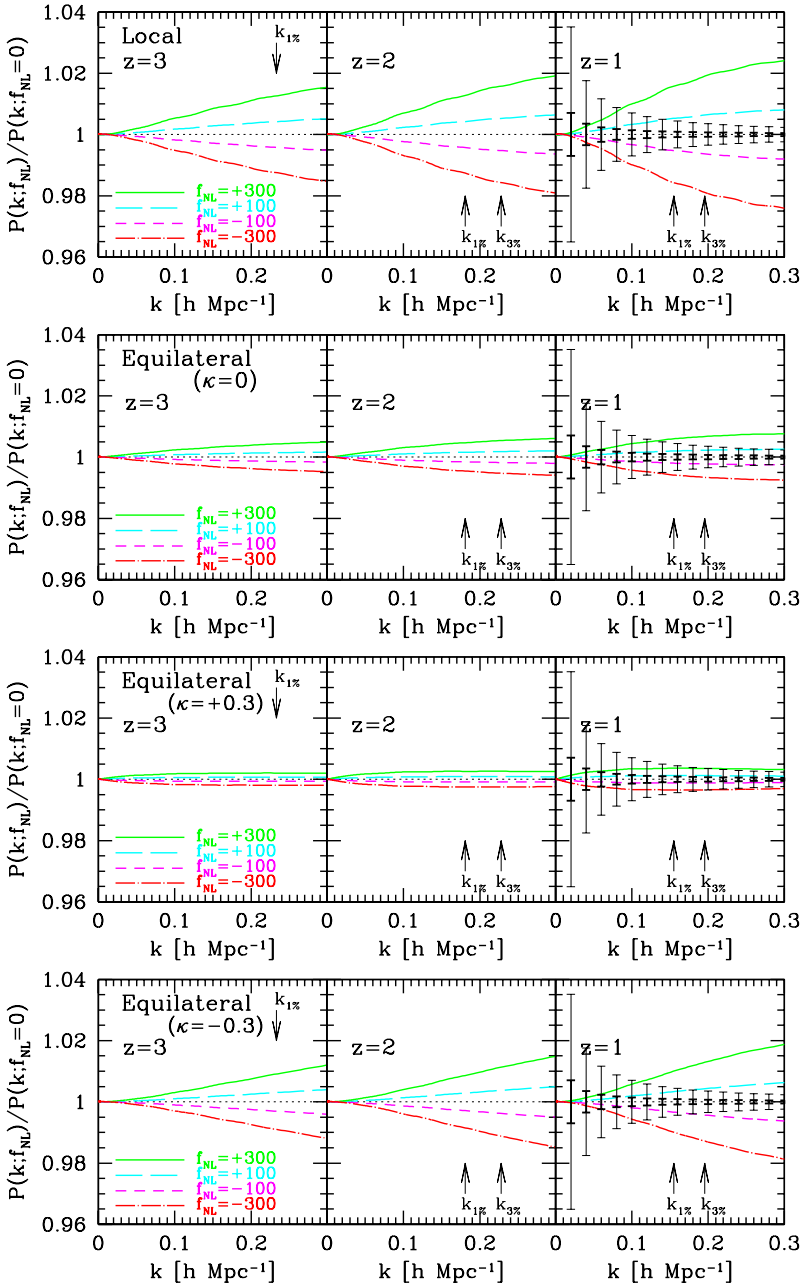


FIG. 2: Ratios of power spectrum, $P(k; f_{\rm NL} \neq 0)/P(k; f_{\rm NL} = 0)$, for $z = 3$ (left), 2 (middle) and 1 (right). From top to bottom panels, the results for the local, equilateral with $\kappa = 0$, 0.3, and $-0.3$ are shown, respectively. In each panel, we plot the cases with non-Gaussian parameter $f_{\rm NL} = +300$ (solid), $+100$ (long-dashed), $-100$ (short-dashed) and $-300$ (dot-dashed). The vertical arrows labeled by $k_{1\%}$ and $k_{3\%}$ indicate the maximum wave number below which the perturbation theory predictions are reliable with a precision of 1% and 3% level, respectively, according to the criteria (3.11) [50]. As references, the error bars limited by the cosmic variance are plotted in the right panel, assuming the survey volume of $V_s = 4\,(h^{-1}{\rm Gpc})^3$ (thin solid) and $V_s = 10^2\,(h^{-1}{\rm Gpc})^3$ (thick solid).

we plot the error bars in each right panel, which represent the expected $1-\sigma$ errors, $\Delta P(k)$, limited by the cosmic-variance, i.e., $\Delta P(k)/P(k) = (2/N_k)^{1/2}$ with $N_k$ being the number of Fourier modes within a given bin at $k$. Here, we specifically consider the two representative cases of $V_{\rm s} = 4\,(h^{-1}{\rm Gpc})^3$ (thin) and $V_{\rm s} = 10^2\,(h^{-1}{\rm Gpc})^3$ (thick), corresponding to the future surveys dedicated for the measurement of baryon acoustic oscillations (BAOs) from the ground and space, respectively. Naively comparing the error bars to the amplitudes of the non-Gaussian effects, ground-based BAO surveys with a typical volume of $V \sim$few $h^{-3}{\rm Gpc}^3$ will find it difficult to detect the signature of primordial non-Gaussianity only from the power spectrum. However, idealistic surveys with huge volumes seem to

show the potential for a definite detection of non-Gaussian effects even with the currently constrained values of $f_{\rm NL}$.

## IV. IMPACT ON COSMOLOGICAL PARAMETER ESTIMATION

### A. Fisher-matrix analysis

Apart from primordial non-Gaussianity, there are several parameters that affect the shape of the power spectrum. Among these, the primordial spectral index $n_s$ and running index $\alpha \equiv dn_s/d\ln k$ monotonically change the power spectrum, which resemble the effect of primordial non-Gaussianity at some wavenumbers. A natural question arises whether the primordial non-Gaussianity is indeed detectable or not considering the degeneracies and how the non-negligible effect of non-Gaussianity adversely affects the estimations of primordial spectral index and the running of the index. On the other hand, for the scales accessible to the future surveys, a measurement of the characteristic scale of BAOs is an important clue to probe the late-time acceleration of the universe e.g., [27, 43, 60]), and a percent-level determination of the acoustic scale is required for the determination of the dark energy equation of state [3, 51]. In this respect, even the small effect of primordial non-Gaussianity may affect the determination of the BAO scale.

Here, we apply the Fisher-matrix method to address these issues and explore the potential impact on cosmological parameter estimation as well as the determination of the BAO scale. For this purpose, we consider a rather simplified setup, namely that our observable is the real-space power spectrum free from the redshift-space distortion. Under the assumption of linear galaxy biasing, the observed power spectrum may be written as (e.g., [30]):

$$P_{\rm obs}(k;z) = \left(\frac{D_V(z)}{D_{V,\rm true}(z)}\right)^3 b_1^2\, P_{\rm mass}\left(\frac{D_{V,\rm true}(z)}{D_V(z)}\,k;\, z\right), \tag{4.1}$$

where the power spectrum $P_{\rm mass}$ is computed from perturbation theory. Here, $b_1$ is the linear biasing parameter, and $D_V(z)$ represents the cosmological distance averaged over three-dimensional space, $D_V(z) \equiv [D_A^2(z)/H(z)]^{1/3}$. The subscript "true" denotes the quantities estimated from the true cosmological model.

Following Refs.[66, 67], the Fisher matrix for the galaxy power spectrum is given by

$$F_{ij} = \frac{V_s}{(2\pi)^2}\int_{k_{\rm min}}^{k_{\rm max}} dk\, k^2\, \frac{\partial \ln P(k;z)}{\partial\theta_i}\frac{\partial \ln P(k;z)}{\partial\theta_j}\left\{\frac{n_{\rm gal}\,P(k;z)}{n_{\rm gal}\,P(k;z)+1}\right\}^2, \tag{4.2}$$

where $\theta_i$ represents one from a set of parameters. The quantity $V_s$ is the survey volume and $n_{\rm gal}$ is the number density of galaxies. The range of integration $[k_{\rm min}, k_{\rm max}]$ should be determined through the survey properties, and in particular the minimum wave number is limited to $2\pi/V_s^{1/3}$. Note that the choice of $k_{\rm min}$ may be crucial for the power spectrum measurement on large-scales $k \lesssim 0.01h{\rm Mpc}^{-1}$, where the scale-dependent effect of galaxy biasing becomes prominent through the non-trivial mode-coupling from primordial non-Gaussianity [2, 19, 42, 46, 62]. Here, we fix $k_{\rm min} = 0.01h{\rm Mpc}^{-1}$ and allow $k_{\rm max}$ to vary. The effect of scale-dependent biasing will be discussed in next section.

In the Fisher-matrix analysis presented below, we include the five parameters given by $\theta_i = \{n_s,\ \alpha,\ D_V/D_{V,\rm true},\ f_{\rm NL},\ b_1\}$. The fiducial values of these parameters are set to $n_s = 0.961$, $\alpha = 0$, $D_V/D_{V,\rm true} = 1$, and $f_{\rm NL} = 0$. We then consider a space-based BAO survey as an idealistically gigantic galaxy survey along the lines of SPACE and ADEPT ([5, 53, 54], see also Ref. [59]). We adopt the survey parameters of a space-based BAO experiment as follows: $z = 1.5$, $V_s = 100\,(h^{-1}{\rm Gpc})^3$, $b_1 = 3.25$, and $n_{\rm gal} = 3.25\times10^{-4}(h^{-1}{\rm Mpc})^{-3}$ (e.g., [59]). Below, we mainly focus on the local model of primordial non-Gaussianity. The results for the equilateral model are qualitatively the same as in the local model and are briefly summarized in Table I.

### B. Results

Figure 3 shows the marginalized 1-$\sigma$ (68%C.L.) errors on the spectral index $n_s$ (left), the running of the index $\alpha$ (middle), and the distance scale $D_V/D_{V,\rm true}$ (right) as function of cutoff scale, $k_{\rm max}$. Here, the solid lines represent the results assuming no prior information to these parameters (*prior 1*, solid). The short- and long-dashed lines correspond to the results taking account of the priors on $n_s$ and $\alpha$, which are expected to come from the upcoming Planck CMB experiment : $\Delta n_s = 0.01$ (*prior 2*, short-dashed); $\Delta n_s = 0.01$ and $\Delta\alpha = 0.002$ (*prior 3*, long-dashed). We assume Gaussian priors for these cases.

Figure 3 indicates that the CMB priors play an important role for the determination of the primordial indices and distance scales. This has been repeatedly pointed out in the literature, but we emphasize that it is indeed crucial when we include the non-Gaussian parameter $f_{\rm NL}$ in the analysis of cosmological parameter estimation. To clarify

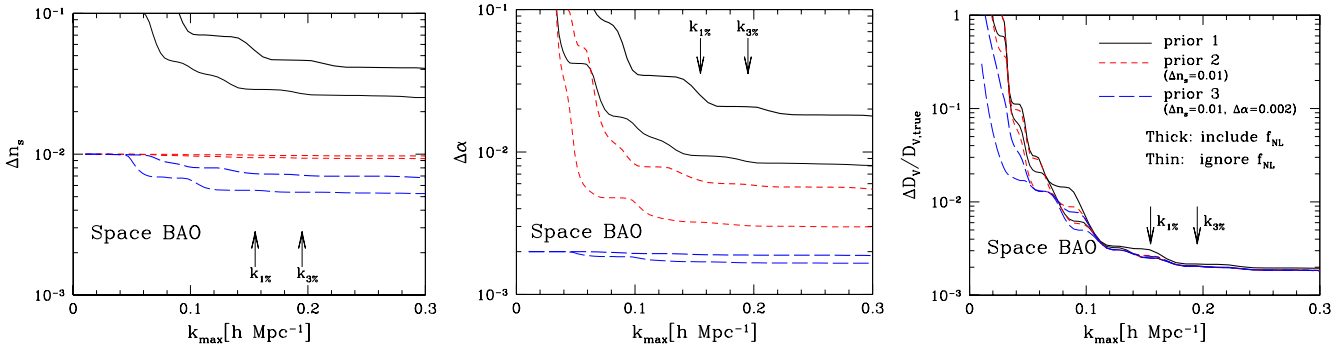


FIG. 3: Predicted 1-$\sigma$ (68%C.L.) errors on the spectral index $n_s$ (left), running of the index $\alpha$ (middle), and distance scale $D_V/D_{V,\rm true}$ (right) as function of maximum wavenumber $k_{\rm max}$, assuming the survey parameters of $z = 1.5$, $V_s = 100h^{-3}{\rm Gpc}^3$, $b_1 = 3.25$, and $n_{\rm gal} = 10^{-4}h^3{\rm Gpc}^{-3}$, as an illustrative example of space-based BAO missions. Here, we specifically treat the local model of primordial non-Gaussianity. The solid (prior 1), short-dashed (prior 2), and long-dashed (prior 3) lines represent the results under the different priors (see text for details). Thick lines show the one-dimensional errors marginalized over the four parameters (i.e., $n_s$, $\alpha$, $D_V/D_{V,\rm true}$, $f_{\rm NL}$), and thin lines represents the error excluding the non-Gaussian parameter, $f_{\rm NL}$.

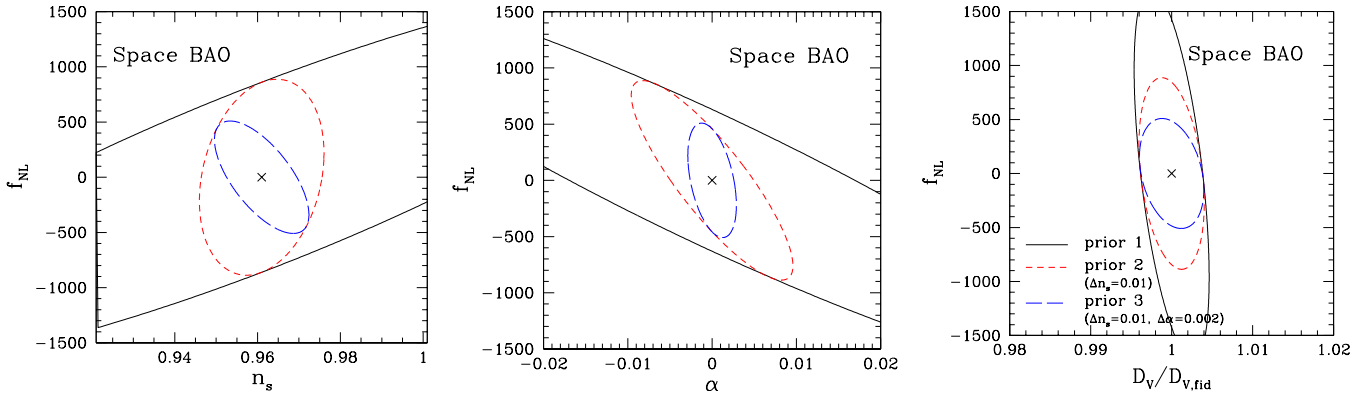


FIG. 4: Two-dimensional joint 68%C.L. constraints on $f_{\rm NL}$ and $n_s$ (left), $\alpha$ (middle), and $D_V/D_{V,\rm true}$ (right), assuming the local model of primordial non-Gaussianity. In deriving the constraints, we fix the maximum wavenumber to $k_{\rm max} = k_{1\%} \simeq 0.155h{\rm Mpc}^{-1}$ and adopt the survey parameters of a space-based BAO mission. The different lines indicate the results from imposing different prior information on $n_s$ and $\alpha$: no priors (solid): $\Delta n_s = 0.01$ (short-dashed): $\Delta n_s = 0.01$, $\Delta\alpha = 0.002$ (long-dashed).

the influences, we exclude $f_{\rm NL}$ from the Fisher-matrix analysis and evaluate the marginalized errors again. The results are plotted in thin lines. Comparing thick with thin lines, we see that the inclusion of the extra parameter $f_{\rm NL}$ significantly worsen the constraints on the primordial index and its running. With strong priors on $n_s$ and $\alpha$ (*prior 3*), tighter constraints comparable to those ignoring primordial non-Gaussianity would be obtained. By contrast, the determination of distance scale $D_V/D_{V,\rm true}$ is insensitive to primordial non-Gaussianity if we choose the cutoff wavenumber $k_{\rm max}$ around $k_{1\%}$, labeled by the vertical arrows. This is partly because the distance scale is mainly determined through the BAOs at linear scales, where the effect of primordial non-Gaussianity becomes negligible at $z \simeq 1.5$. It is interesting to note that all the curves depicted in Figure 3 become almost constant at $k \gtrsim k_{1\%} \simeq 0.155h{\rm Mpc}^{-1}$. Since this scale is slightly larger than the one inferred from the mean separation of galaxies ($n_{\rm gal}^{1/3} \simeq 0.07h{\rm Mpc}^{-1}$), the constancy of the predicted errors implies that the shot-noise contribution becomes significant at $k \gtrsim k_{1\%}$.

In Figure 4, we next plot the two-dimensional constraints on the non-Gaussian parameter $f_{\rm NL}$ and one of the free parameters $n_s$, $\alpha$ and $D_V/D_{V,\rm true}$, marginalizing over the other remaining parameters. In this plot, the cutoff scale is fixed to $k_{\rm max} = k_{1\%}$, and the 1-$\sigma$ (68%C.L.) contours are shown for the three different priors. As expected from Figure 3, the primordial index $n_s$ and its running $\alpha$ without CMB priors (*prior 1*) exhibit a strong degeneracy with the $f_{\rm NL}$ parameter, while the degeneracy between $f_{\rm NL}$ and distance scale is very weak. The uncertainty in the $f_{\rm NL}$ parameter is therefore very large in this case. The errors can be reduced significantly when the strong constraints on $n_s$ and $\alpha$ are obtained (*prior 3*). However, the uncertainty in $f_{\rm NL}$ is still $\Delta f_{\rm NL} \sim 500$, which is quite a bit larger

than other observational techniques using the bispectrum or cluster abundance [39, 57, 59]. The uncertainty may be reduced if we increase the cutoff scale $k_{\rm max}$, although it is generally difficult to accurately predict the power spectrum at these scales, including the higher-order corrections. Hence, it is difficult to detect the non-Gaussian signals even from an idealistic large-volume survey.

Table I summarizes the results of the one-dimensional marginalized errors for various cases with different fiducial values, including the case of the equilateral model. Here, in addition to the priors on $n_s$ and $\alpha$ (*prior 3*), we further put a Gaussian prior on $\kappa$ with $\Delta\kappa = 0.5$, the reason for which comes from the fact that $\kappa$ is the slow-roll parameter and should be restricted to $\kappa \ll 1$. Because of the additional parameter, the resultant errors on $f_{\rm NL}$ significantly increase for the equilateral model, especially with $\kappa > 0$. By contrast, the errors on $n_s$, $\alpha$ and distance scale are hardly affected.

Finally, as a representative example for a more near-term project, we consider the case of a ground-based BAO survey. The survey parameters we adopt are $z = 1$, $V_s = 4\,(h^{-1}{\rm Gpc})^3$, $b_1 = 2$, and $n_{\rm gal} = 10^{-3}\ (h^{-1}{\rm Mpc})^{-3}$ ([5, 22], see also [59]). Figure 5 shows the expected one-dimensional error on $D_V/D_{V,{\rm true}}$ (left) and the two-dimensional errors on $f_{\rm NL}$ and $D_V/D_{V,{\rm true}}$ (right). Compared to the large volume of a space-based BAO experiment, the statistical errors of the measurement of the power spectrum are somewhat larger and thereby the precision of the distance-scale estimation is rather degraded. Nevertheless, the results are hardly affected by the primordial non-Gaussianity.

In conclusion, the presence of primordial non-Gaussianity potentially affects the estimation of the primordial index and the running, and the CMB-based priors on these parameters would be crucial, but the distance-scale measurement is relatively insensitive to it for the appropriate choice of $k_{\rm max}$. In the end, the primordial non-Gaussianity is hardly detectable from galaxy redshift surveys even with idealistically large survey-volume.

## V. ON THE LOCAL BIASING PRESCRIPTION FOR GALAXY POWER SPECTRUM

So far, we have mainly dealt with the matter power spectrum and the galaxy power spectrum has been only considered under the simplified assumption of linear galaxy biasing. In reality, the statistical relation between galaxy and mass is generally complicated due to the non-linear nature of galaxy formation processes, and the linear biasing prescription would not hold even at large scales accessible to the future galaxy surveys.

Although the extension of the linear biasing prescription to include non-linear effects is rather non-trivial, a straightforward and frequently used prescription for galaxy biasing, coupled to perturbation theory, is the local biasing [21], in which the galaxy density field $\delta_{\rm gal}$ at a given position $\boldsymbol{x}$ is described as the local function of mass density field at the same position, i.e., $\delta_{\rm gal}(\boldsymbol{x}) = f[\delta(\boldsymbol{x})]$. On large scales of our interest, this can be expressed as the Taylor series expansion:

$$\begin{aligned}\delta_{\rm gal}(\boldsymbol{x}|R) \;&=\; f[\delta(\boldsymbol{x}|R)] = b_1\,\delta(\boldsymbol{x}|R) + \frac{b_2}{2}\left\{\,[\,\delta(\boldsymbol{x}|R)\,]^2 - \left\langle\,[\delta(\boldsymbol{x}|R)]^2\,\right\rangle\right\} \\ &\quad + \frac{b_3}{3!}\left\{\,[\,\delta(\boldsymbol{x}|R)\,]^3 - \left\langle\,[\delta(\boldsymbol{x}|R)]^3\,\right\rangle\right\} + \cdots\,, \end{aligned} \tag{5.1}$$

where the quantities $\delta_{\rm gal}(\boldsymbol{x}|R)$ and $\delta(\boldsymbol{x}|R)$ are the galaxy and mass density fields smoothed over the radius $R$ centered at the position $\boldsymbol{x}$. In the above expression, the coefficients $b_2$ and $b_3$ describe the non-linearity of galaxy biasing, which

TABLE I: Marginalized one-dimensional errors (68%C.L.) on $n_s$, $\alpha$, $D_V/D_{V,{\rm true}}$ and non-Gaussian parameters $f_{\rm NL}$ and $\kappa$ from Fisher-matrix analysis adopting the survey parameters of a space-based BAO experiment

| Fiducial model | $\Delta n_s$ | $\Delta\alpha$ | $\Delta(D_V/D_{V,{\rm true}})$ | $\Delta f_{\rm NL}$ | $\Delta\kappa^\dagger$ |
|---|---|---|---|---|---|
| Local ($f_{\rm NL}=0$) | 0.0075 | 0.0019 | 0.0026 | 335 | — |
| Local ($f_{\rm NL}=+100$) | 0.0075 | 0.0019 | 0.0026 | 338 | — |
| Equilateral ($f_{\rm NL}=+250,\ \kappa=-0.3$) | 0.0072 | 0.0019 | 0.0025 | 596 | 0.48 (0.37) |
| Equilateral ($f_{\rm NL}=+250,\ \kappa=0$) | 0.0086 | 0.0020 | 0.0025 | 1306 | 0.48 (0.45) |
| Equilateral ($f_{\rm NL}=+250,\ \kappa=+0.3$) | 0.0082 | 0.0018 | 0.0025 | 2774 | 0.49 (0.49) |
| Equilateral ($f_{\rm NL}=-150,\ \kappa=-0.3$) | 0.0071 | 0.0019 | 0.0025 | 498 | 0.49 (0.43) |
| Equilateral ($f_{\rm NL}=-150,\ \kappa=0$) | 0.0085 | 0.0020 | 0.0025 | 1230 | 0.49 (0.48) |
| Equilateral ($f_{\rm NL}=-150,\ \kappa=+0.3$) | 0.0082 | 0.0018 | 0.0025 | 2753 | 0.50 (0.50) |

$^\dagger$ parentheses represent the marginalized 1-$\sigma$ error when further adopting the Gaussian prior of $\Delta f_{\rm NL} = 75$

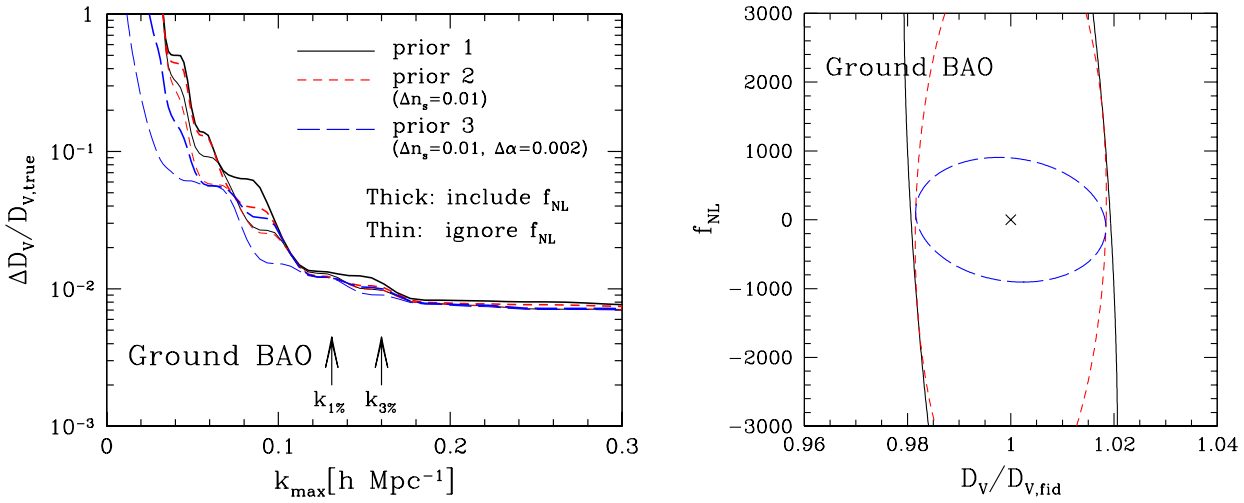


FIG. 5: Expected 1-$\sigma$ (68%C.L.) error on the distance scale as a function of maximum wavenumber (left) and two-dimensional joint 68% C.L. constraints on $f_{\rm NL}$ of the local model and $D_V/D_{V,\rm true}$ fixing the maximum wavenumber to $k_{\rm max} = k_{1\%} \simeq 0.131h{\rm Mpc}^{-1}$ (right). Here, we specifically adopt the survey parameters of $z = 1$, $V_s = 4\,h^{-3}{\rm Gpc}^3$, $b_1 = 2.0$, and $n_{\rm gal} = 10^{-3}$ $h^3{\rm Mpc}^{-3}$, as a representative example of ground-based BAO surveys. The meaning of the lines are the same as in Figures 3 and 4.

are incorporated into the galaxy power spectrum $P_{\rm gal}(k)$, through the perturbative calculation of the matter power spectrum ([24, 45, 63], see also [44, 65] for different parametrization schemes). Although the relation (5.1) is just a phenomenological prescription, it has been recently applied to the characterization of the BAOs, and the model of galaxy power spectra has been tested against numerical simulations of halo/galaxy clustering in the case of Gaussian initial condition [31, 63].

When we consider primordial non-Gaussianity, several non-trivial corrections to the galaxy power spectrum $P_{\rm gal}(k)$ appears, which can further alter the shape of the power spectrum on large scales. This has been first pointed out by McDonald [46]. Here, we rephrase his finding and advocate its observational importance, together with potential problems.

Let us focus on the scales larger than the characteristic scale of BAOs, above which the higher-order perturbations can be safely neglected. Collecting the relevant terms in the expansion (5.1), the power spectrum of the galaxy density fields smoothed over the radius $R$ may be expressed as

$$P_{\rm gal}(k;z|R) = b_1^2 \left\{ D^2(z)P_0(k) + P^{(12)}(k;z) \right\} W^2(kR) + b_1 b_2\, F(k;z,f_{\rm NL}|R) + \cdots , \tag{5.2}$$

up to the third-order in mass density field, i.e., $\mathcal{O}(\delta_0^3)$. Here, $W(x)$ is the filter function defined in Fourier space. In equation (5.2), there are two types of non-Gaussian contributions. One is the term $P^{(12)}(k;z)$ coming from the matter power spectrum, and the other is the function $F(k;z,f_{\rm NL})$ arising from the non-linear mapping of the galaxy biasing. The explicit expression of the function $F$ is

$$\begin{aligned} F(k;z,f_{\rm NL}|R) = D^3(z) \int \frac{d^3q}{(2\pi)^3}\, & M_\zeta(k) M_\zeta(q) M_\zeta(|\boldsymbol{k}-\boldsymbol{q}|) \\ & \times W(kR) W(qR) W(|\boldsymbol{k}-\boldsymbol{q}|R)\, B_\zeta(-\boldsymbol{k},\boldsymbol{q},\boldsymbol{k}-\boldsymbol{q}). \end{aligned} \tag{5.3}$$

The functional form of $F$ is clearly different from the perturbative corrections of the matter power spectrum, $P^{(12)}$ (Eq.(3.5) or (3.8) ). Hence, the presence of this term potentially leads to the scale-dependent galaxy biasing, relative to the matter power spectrum.

Before continuing, we note that the quantity $P_{\rm gal}(k;z|R)$ manifestly depends on the smoothing radius $R$. In the usual sense, $P_{\rm gal}(k;z|R)$ would not be directly related to the power spectrum derived from the unfiltered observations. It has been put forward in Ref. [63] that the unfiltered galaxy power spectrum $P_{\rm gal}(k;z)$ can be recovered through the simple operation:

$$P_{\rm gal}(k;z) = \frac{P_{\rm gal}(k;z|R)}{W^2(kR)}. \tag{5.4}$$

While the above definition still includes the smoothing radius, we regard equation (5.4) as a direct observable and evaluate it with the appropriate smoothing radius to see what happens. Below, we will separately treat the galaxy power spectra for the local and equilateral models of primordial non-Gaussianity.

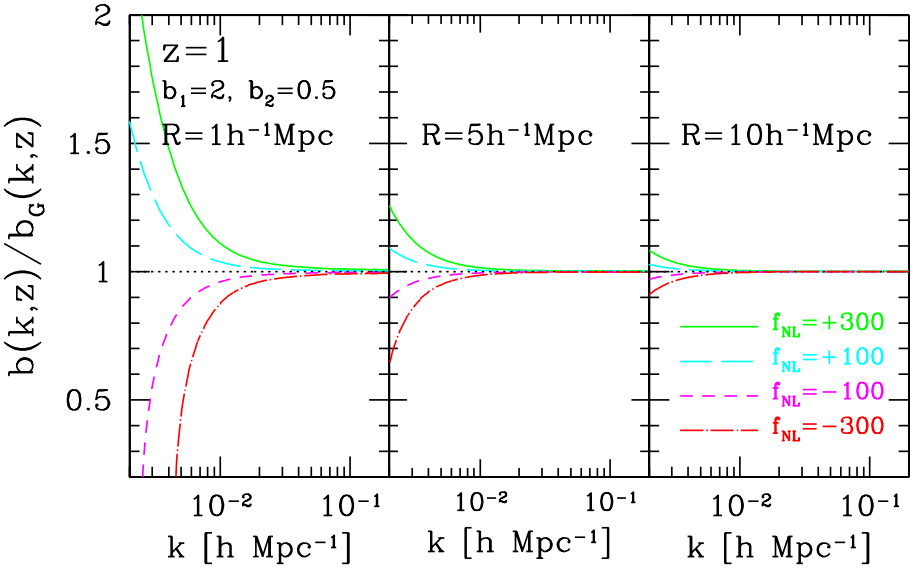


FIG. 6: Ratio of biasing factor, $b(k;z)/b_{\rm G}(k;z)$ given at $z=1$, in the case of the local model. Gaussian smoothing is adopted in order to compute the biased power spectra. $R=1h^{-1}$Mpc (left); $R=5h^{-1}$Mpc (middle); $R=10h^{-1}$Mpc (right)

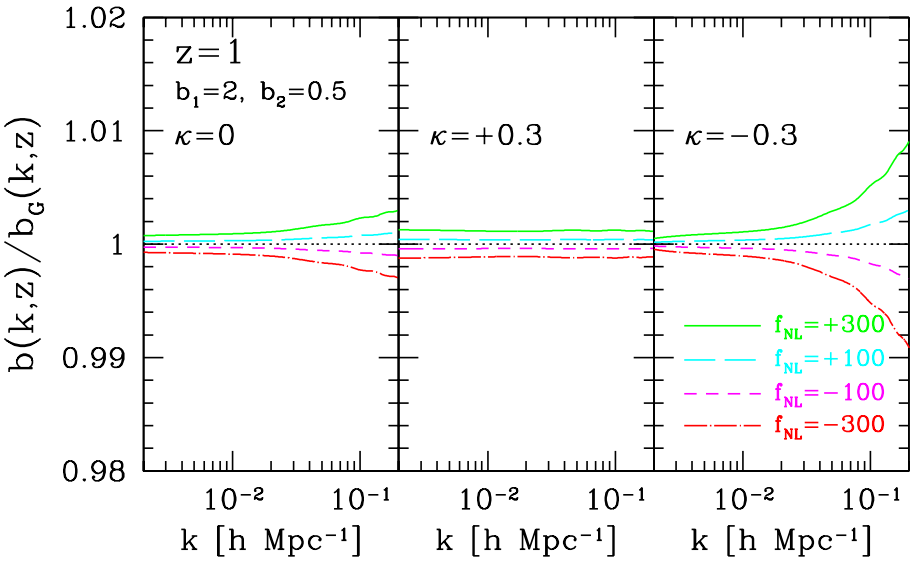


FIG. 7: Ratio of biasing factor, $b(k;z)/b_{\rm G}(k;z)$, given at $z=1$ in the case of the equilateral model. In this plot, we do not consider Gaussian smoothing. $\kappa=0$ (left); $\kappa=0.3$ (middle); $\kappa=-0.3$ (right).

### A. Local model

Figures 6 plots the ratio of the biasing factor, $b(k;z)/b_{\rm G}(k;z)$, plotted against the wavenumber, in the case of local model. Here, the biasing factor $b(k;z)$ is defined by

$$b(k;z)\equiv\left\{\frac{P_{\rm gal}(k;z)}{P_{\rm mass}(k;z)}\right\}^{1/2}. \tag{5.5}$$

The function $b_{\rm G}(k;z)$ is similarly defined as above, but with $f_{\rm NL}=0$. For illustrative purposes, we specifically set the biasing coefficients to $b_1=2$ and $b_2=0.5$, and the results for $z=1$ are shown for different values of non-Gaussian parameter $f_{\rm NL}$. Three different panels show the dependence of the smoothing radius, adopting Gaussian smoothing, $W(x)=\exp(-x^2/2)$, with radii $R=1h^{-1}$Mpc (left), $5h^{-1}$Mpc (middle), and $10h^{-1}$Mpc (right).

Clearly, the ratios of the biasing factor exhibit a strong scale-dependence, especially at $k\lesssim 0.01h{\rm Mpc}^{-1}$. Note that the function $F$ logarithmically diverges unless we introduce a large smoothing radius $R$. Accordingly, the strength of the scale-dependence sensitively depends on $R$ as well as $f_{\rm NL}$. The origin of this scale-dependence can be deduced from a simple manipulation as follows. Substituting the bispectrum of the local model (2.10) into the expression (5.2), we take the limit $k\to 0$. The correction $P^{(12)}(k)$ becomes negligibly small, and the term including the function $F$ is the only dominant contribution to the galaxy power spectrum. We have

$$F(k;z,f_{\rm NL}|R)\simeq\frac{12}{5}\,f_{\rm NL}\,D^3(z)\,P_0(k)\,\frac{W(kR)\sigma^2(R)}{M_\zeta(k)};\qquad \sigma^2(R)=\int\frac{d^3q}{(2\pi)^3}\,W^2(qR)P_0(q), \tag{5.6}$$

where we used the fact that the function $M_\zeta(k)$ defined in equation (2.2) asymptotically behaves like $M_\zeta\propto k^2$ ($k^0$) in the limit of $k\to 0$ ($k\to\infty$). Here, the quantity $\sigma(R)$ represents the rms amplitude of the linear density fluctuation $\delta_0$. Then, from (5.4) and (5.5), we obtain

$$b(k;z)\simeq b_1\left[1+\frac{12}{5}f_{\rm NL}\,\frac{b_2}{b_1}D(z)\frac{\sigma^2(R)}{M_\zeta(k)W(kR)}\right]^{1/2}. \tag{5.7}$$

The expression (5.7) contains a term inversely proportional to $M_\zeta(k)$, which leads to the strong scale-dependence at $k\to 0$. Now, we recognize the fact that the scale-dependence of the biasing factor depends not only on $R$ and $f_{\rm NL}$, but also on the ratio of biasing coefficients, $b_2/b_1$, and redshift, $z$.

It is interesting to note that similar kinds of behavior can be found in the halo biasing prescription [2, 19, 42, 62]. While the halo biasing describes the clustering properties of virialized objects based on the Press-Schechter theory, the origin of the scale-dependence is qualitatively the same as that of the local biasing mentioned above. In this sense, the scale-dependent biasing may be a unique character of the local model of primordial non-Gaussianity and it would be an important observable of the large-scale structure.

Note, however, that the scale-dependent biasing factor in the local biasing seems problematic because of the logarithmic divergence at $R\to 0$, which originates from the rms amplitude $\sigma(R)$ in the case of a CDM power spectrum. Further, the biasing factor $b(k;z)$ can be ill-defined for the negative $f_{\rm NL}$ or $b_2$ and it eventually becomes complex at $k\to 0$. McDonald [46] proposed a renormalization treatment to remove these difficulties by adding a non-local counter term to the relation (5.1). Although the addition of a counter term might be a possible solution, uniqueness of this treatment seems is unclear, and thus the physical reason for the non-local counter term is unclear. In fact, as shown in next subsection, the scale-dependence of the biasing factor turns out to be model-dependent, and the logarithmic divergence disappears when we consider the equilateral model of primordial non-Gaussianity.

### B. Equilateral model

In Figure 7, we plot the ratio of the biasing factor, $b(k;z)/b_{\rm G}(k;z)$, in the equilateral model. Here, instead of showing the dependence of smoothing radius, we neglect the effect of smoothing (i.e., $R\to 0$) and just examine the effect of scale-dependent non-Gaussianity by changing $\kappa$ to 0 (left), $-0.3$ (middle) and 0.3 (right).

In marked contrast to the local model, it turns out that the biasing factors $b(k;z)$ in the equilateral model are almost constant on large scales, and the linear deterministic biasing, $P_{\rm gal}(k)=b_1^2P_{\rm mass}(k)$, is an excellent approximation to the galaxy power spectrum on large scales. These features are irrespective of the values of $\kappa$, and can be deduced from the asymptotic behavior of the function $F$. In the $k\to 0$ limit, we have

$$\begin{aligned}F(k;z,f_{\rm NL}|R=0)\;\simeq\;&\frac{18}{5}\,f_{\rm NL}\,D^3(z)\,M_\zeta(k)\\&\times\int\frac{d^3q}{(2\pi)^3}\left(\frac{2q/3}{k_{\rm CMB}}\right)^{-2\kappa}\{M_\zeta(q)\}^2\left[2\left\{P_\zeta(k)P_\zeta^5(q)\right\}^{1/3}-\left\{P_\zeta(q)\right\}^2\right].\end{aligned} \tag{5.8}$$

Recalling the power-law nature of the primordial spectrum $P_\zeta(q)\propto q^{n_s-4}$, the integral in the above equation converges if $n_s\sim 1$ and $|\kappa|\lesssim 0.3$. As a result, the function $F$ scales as $F(k;z,f_{\rm NL}|R=0)\propto M_\zeta(k)\propto k^2$ and the non-Gaussian contribution becomes negligibly smaller than the linear biasing term, $b_1^2P_{\rm mass}(k;z)$.

Therefore, as long as the equilateral model of primordial non-Gaussianity is concerned, it is hard to constrain $f_{\rm NL}$ through the scale-dependent biasing factor. Although this conclusion comes from the assumption of the local biasing

prescription, this would generally hold for other biasing schemes, including the halo biasing prescription. On the other hand, a big difference in the scale-dependent biasing factor between the local and equilateral models implies that the galaxy biasing is very sensitive to the shape of the primordial bispectrum. An essential reason for having a scale-dependent biasing only for the local-type primordial non-Gaussianity is that the amplitude of the primordial bispectrum with squeezed configuration, i.e., $B_\zeta(-\boldsymbol{k}, \boldsymbol{q}, \boldsymbol{k}-\boldsymbol{q})$ with $|\boldsymbol{k}| \ll |\boldsymbol{q}|$, is greater than that of the equilateral case (see Eq.(5.3)). The local-type primordial non-Gaussianity has fairly strong mode-correlations between small and large Fourier modes, and thereby the biasing, as a small-scale phenomenon, affects the power spectrum on very large scales. This generic feature might be very helpful to discriminate between the types of primordial non-Gaussianity. The detection of scale-dependent biasing may have interesting implication for the inflationary model, according to the single-field consistency relation [16]. The consistency relation states that as long as the inflation dynamics is driven by a single scalar field, the primordial bispectrum in squeezed configuration becomes very small, irrespective of the type of non-Gaussianity. Thus, single-field inflation generically predicts scale-independent biasing on large scales. Therefore, if the presence of scale-dependent biasing on large scales is observationally verified, this strongly disproves the consistency relation, and the inflation dynamics may not be simply characterized by the single scalar field.

## VI. DISCUSSION AND CONCLUSIONS

In this paper, we have comprehensively studied the effect of primordial non-Gaussianity on the power spectrum of large-scale structure. Using perturbation theory, we calculate the leading-order non-Gaussian corrections to the matter power spectrum through the non-linear mode coupling of the gravitational evolution. In the weakly non-linear regime, the signature of primordial non-Gaussianity in the matter power spectrum can be characterized by the primordial bispectrum. Adopting two representative models of the bispectrum (local and equilateral), we quantitatively estimate the non-Gaussian signals on the matter power spectrum. The primordial non-Gaussianity systematically enhances or suppresses the non-linear growth of the power spectrum amplitude at the $\lesssim$ 1-2% level.

We then explore the potential impact on the cosmological parameter estimations from future dedicated surveys for BAO measurement. Under the assumption of scale-independent linear biasing, the Fisher-matrix analysis reveals that while it is hard to detect the primordial non-Gaussianity to the level of current constraints, the inclusion of the non-Gaussian parameter $f_{\rm NL}$ significantly degrades the constraints on the primordial spectral index $n_s$ and the running of the index $\alpha$. In this respect, the CMB prior information for $n_s$ and $\alpha$ as well as the non-Gaussian parameter is very crucial. On the other hand, determination of the distance scale $D_A(z)$ is rather insensitive to the presence or absence of primordial non-Gaussianity, and thus the characteristic scale of BAOs is a robust standard ruler.

We have also considered the effects of primordial non-Gaussianity on the galaxy biasing. In the framework of local galaxy biasing, in which the number density of galaxies is described by a local function of the mass density field, we found that the non-linear mapping of galaxy biasing can modulate the power spectrum and this sensitively depends on the shape of non-Gaussianity. In the local model of primordial non-Gaussianity, mode-correlations between large scales and small scales are fairly strong, and the non-Gaussian correction induces the strong scale-dependent biasing on large-scales, while the scale-independent linear biasing is preserved to a good accuracy in the equilateral model. These remarkable properties may be very helpful in discriminating between the types of primordial non-Gaussianity, especially in connection with the single-field consistency relation. However, the biasing factor in the local model exhibits an apparent divergence, suggesting that the local biasing prescription may be incompatible with the local model of primordial non-Gaussianity. Indeed, the local biasing scheme is just a phenomenological parametrization and the validity of this prescription itself has not yet been tested enough in the presence of non-Gaussianity. Further study using simulations is necessary for quantitative prediction of the non-Gaussian signature on galaxy biasing.

### Acknowledgments

We would like to thank Patrick McDonald and Shun Saito for comments and discussion, and Erik Reese for a careful reading of the manuscript. AT is supported by a Grant-in-Aid for Scientific Research from the Japan Society for the Promotion of Science (JSPS) (No. 18740132). TM acknowledges support from the Ministry of Education, Culture, Sports, Science, and Technology, Grant-in-Aid for Scientific Research (C) (No. 18540260, 2006). KK is supported by STFC and RCUK. This work was supported in part by Grant-in-Aid for Scientific Research on Priority Areas No. 467 “Probing the Dark Energy through an Extremely Wide and Deep Survey with Subaru Telescope”, and JSPS

Core-to-Core Program "International Research Network for Dark Energy".

---


[1] V. Acquaviva, N. Bartolo, S. Matarrese, and A. Riotto, Nucl.Phys.B **667** (2003) 119.
[2] N. Afshordi and A. J. Tolley, arXiv:0806.1046 [astro-ph].
[3] A. Albrecht. et al. astro-ph/0609591.
[4] M. Alishahiha, E. Silverstein, and D. Tong, Phys.Rev.D **70** (2004) 123505.
[5] A. Albrecht et al., astro-ph/0609591.
[6] F. Arroja and K. Koyama, Phys. Rev. D **77**, 083517 (2008)
[7] F. Arroja, S. Mizuno, and. K. Koyama, J.Cosmol.Astropart.Phys. **08** (2008) 015.
[8] H. Assadullahi, J. Valiviita, and D. Wands, Phys. Rev. D **76**, 103003 (2007)
[9] D. Babich, P. Creminelli, and M. Zaldarriaga, J.Cosmol.Astropart.Phys. **08** (2004) 009.
[10] J. Bardeen, Phys.Rev.D **22** (1980) 1882.
[11] N. Bartolo, E. Komatsu, S. Matarrese, and A. Riotto, Phys.Rep. **420** (2004) 103.
[12] F. Bernardeau, S. Colombi, E. Gaztanaga, and R. Scoccimarro, Phys. Rep. **367** (2002) 1.
[13] E. I. Buchbinder, J. Khoury, and B. A. Ovrut, Phys. Rev. Lett. **100**, 171302 (2008)
[14] C. Carbone, L. Verde, and S. Matarrese, Astrophys.J. **684** (2008) L1.
[15] X. Chen, M. x. Huang, S. Kachru, and G. Shiu, JCAP **0701**, 002 (2007).
[16] P. Creminelli and M. Zaldarriaga, J.Cosmol.Astropart.Phys. **10** (2004) 006.
[17] P. Creminelli, L. Senatore, M. Zaldarriaga, and M. Tegmark, J.Cosmol.Astropart.Phys. **3** (2007) 005.
[18] P. Creminelli and L. Senatore, J.Cosmol.Astropart.Phys. **11** (2007) 010.
[19] N. Dalal, O. Doré, D. Huterer, and A. Shirokov, Phys.Rev.D**77** (2008) 123514.
[20] D. J. Eisenstein and W. Hu, Astrophys.J. **496** (1998) 505.
[21] J. N. Fry and E. Gaztañaga, Astrophys.J. **413** (1993) 447.
[22] K. Glazebrook et a l. astro-ph/0507457.
[23] M. Grossi, E. Branchini, K. Dolag, S. Matarrese, and L. Moscardini, Mon.Not.Roy.Astron. **390** (2008) 438.
[24] A. Heavens, L. Verde, and S. Matarrese, Mon.Not.Roy.Astron. **301** (1998) 797.
[25] C. Hikage, E. Komatsu, and T. Matsubara, ApJ **653** (2006) 11.
[26] C. Hikage, T. Matsubara, P. Coles, M. Liguori, F. K. Hansen, S. Matarrese, Mon.Not.Roy.Astron. **389** (2008) 1439.
[27] W. Hu and Z. Haiman, Phys.Rev.D **68** (2003) 063004.
[28] M. x. Huang and G. Shiu, Phys. Rev. D **74**, 121301 (2006).
[29] B. Jain and E. Bertschinger, Astrophys.J. **431** (1994) 495.
[30] D. Jeong and E. Komatsu, Astrophys.J. **651** (2006) 619.
[31] D. Jeong and E. Komatsu, arXiv:0805.2632 [astro-ph].
[32] J. Khoury, B. A. Ovrut, P. J. Steinhardt, and N. Turok, Phys. Rev. D **64** (2001) 123522.
[33] E. Komatsu et al., arXiv:0803.0547 [astro-ph].
[34] K. Koyama, S. Mizuno, F. Vernizzi, and D. Wands, J.Cosmol.Astropart.Phys. **11** (2007) 024.
[35] D. Langlois, S. Renaux-Petel, D. A. Steer, and T. Tanaka, arXiv:0806.0336 [hep-th]; arXiv:0804.3139 [hep-th].
[36] J. L. Lehners and P. J. Steinhardt, Phys. Rev. D **77**, 063533 (2008); Phys. Rev. D **78**, 023506 (2008).
[37] D. H. Lyth and D. Wands, Phys.Lett. B **524** (2002) 5.
[38] D. H. Lyth and Y. Rodriguez, Phys.Rev.Lett. **95** (2005) 121302.
[39] M. LoVerde, A. Miller, S. Shandera, and L. Verde, J.Cosmol.Astropart.Phys. **04** (2008) 014.
[40] N. Makino, M. Sasaki, and Y. Suto, Phys.Rev.D **46** (1992) 585.
[41] J. M. Maldacena, JHEP **05** (2003) 013; S. Matarrese and L. Verde, Astrophys.J. **677** (2008) L77.
[42] S. Matarrese and L. Verde, Astrophys.J. **677** (2008) L77.
[43] T. Matsubara, Astrophys.J. **615** (2004) 573.
[44] T. Matsubara, Phys.Rev.D **78** (2008) 083519; *ibid.* **78** (2008) 109901(E).
[45] P. McDonald, Phys.Rev.D **74** (2006) 103512.
[46] P. McDonald, arXiv:0806.1061 [astro-ph].
[47] J. D. McEwen, M. P. Hobson, A. N. Lasenby, and D. J. Mortlock, Mon.Not.Roy.Astron. **388** (2008) 659.
[48] T. Moroi and T. Takahashi, Phys.Lett. B **522** (2001) 215.
[49] T. Nishimichi et al. Publ.Astron.Soc.Japan **59** (2007) 1049.
[50] T. Nishimichi et al. Publ.Astron.Soc.Japan **59** (2008) in press (arXiv:0810.0813 [astro-ph]).
[51] J. A. Peacock et al. astro-ph/0610906.
[52] `http://www.rssd.esa.int/index.php?project=PLANCK&page=index`
[53] M. Robberto, et al. arXiv:0710.3970 [astro-ph].
[54] `http://universe.nasa.gov/program/probes/adept.html`
[55] M. Sasaki, J. Väliviita, and D. Wands, Phys.Rev.D **74** (2006) 103003.
[56] R. Scoccimarro and J. Frieman, Astrophys.J. **473** (1996) 620.
[57] R. Scoccimarro, E. Sefusatti, and M. Zaldarriaga, Phys.Rev.D **69** (2004) 103513.
[58] D. Seery and J. E. Lidsey, J.Cosmol.Astropart.Phys. **06** (2005) 003.

[59] E. Sefusatti and E. Komatsu, Phys.Rev.D **76** (2007) 083004.
[60] H-J. Seo and D. Eisenstein, Astrophys.J. **598** (2003) 720.
[61] P. Serra and A. Cooray, Phys.Rev.D **77** (2008) 107305.
[62] A. Slosar, C. Hirata, U. Seljak, S. Ho, and N. Padmanabhan, J.Cosmol.Astropart.Phys. **08** (2008) 031.
[63] R. E. Smith, R. Scoccimarro, and R. K. Sheth, Phys.Rev.D **75** (2007) 063512.
[64] Y. Suto and M. Sasaki, Phys.Rev.Lett. **66** (1991) 264.
[65] A. Taruya, Astronphys.J. **537** (2000) 37.
[66] M. Tegmark, A. N. Taylor, A. Heavens, ApJ. **48** (1997) 22.
[67] M. Tegmark, Phys.Rev.Lett. **79** (1997) 3806.
[68] M. Tegmark, et al., Phys.Rev.D **74** (2006) 123507.
[69] A. P. S. Yadav and B. D. Wandelt, Phys.Rev.Lett. **100** (2008) 181301.